Multiband Acoustic-Wave-Lumped-Element Resonator-Based Bandpass-to-Bandstop Filters

Nikolaus S. Luhrs, *Student Member, IEEE*, Dakotah J. Simpson, *Student Member, IEEE*, and Dimitra Psychogiou, *Member, IEEE*

***Abstract*— A new class of multiband acoustic-wave resonator-based RF filters with reconfigurable bandpass-to-bandstop (BP-to-BS) transfer function characteristics is reported. They are based on a hybrid integration scheme in which multiresonant acoustic-wave-lumped-element-resonators (AWLRs) are combined with five static and one switched impedance inverters. Each multiresonant AWLR controls the number of bands and their center frequencies. Switching between the bandpass and bandstop modes of operation is achieved by changing the coupling path between its input/output ports through an RF-switched impedance inverter. For practical validation purposes, two prototypes were designed, manufactured, and tested. They include a single-band BP-to-BS filter at 418 MHz and a dual-band BP-to-BS filter with bands centered at 418 and 433.9 MHz.**

***Index Terms*— Acoustic-wave filter, bandpass filter (BPF), bandstop filter (BSF), multiband filter, reconfigurable filter, surface-acoustic-wave (SAW) filter.**

I. Introduction

ACOUSTIC-WAVE resonator (AWR)-based filters, such as those based on surface-acoustic-wave (SAW) and bulk-acoustic-wave (BAW) phenomena, have been identified as the most suitable preselect RF filtering technology for the front-end stages of wireless communication transceivers due to their stringent requirements for size compactness and high RF performance—e.g., low insertion loss (IL), high selectivity, and linearity—[1]. Whereas AWRs exhibit quality factors on the order of a thousand, their fractional bandwidth (FBW) is limited to 0.4–0.8k_t^2—k_t^2 is the electromechanical coupling coefficient—when used in conventional ladder, lattice, or self-cascade configurations due to their tightly coupled resonance and antiresonance [2]. Hybrid integration schemes in which AWRs are effectively combined with lumped elements in acoustic-wave-lumped-element resonator (AWLR) arrangements have recently demonstrated the potential to design RF filters with FBWs $> k_t^2$ while exhibiting effective quality factors $Q_{\text{effs}} > 5000$ [3]. They have facilitated the realization of diverse types of transfer functions, including quasi-elliptic bandpass filter (BPF)-type and reflective and absorptive bandstop filter (BSF)-type ones [3], [4]. However, none of the aforementioned concepts addresses the need for RF front-ends with the ability to adjust their operation in complex RF environments which may require multichannel selection or broad spectrum acquisition in the presence of multiple interfering signals.

Taking into consideration the aforementioned needs, this letter presents a new class of AWLR-based filters with a reconfigurable bandpass-to-bandstop (BP-to-BS) transfer function as enabling elements of next generation RF front-ends with multiband and interference-suppression capabilities. The proposed concept is not only smaller than conventional RF-switched filter banks, but it can also be extended to theoretically infinite number of bands while using less filter elements. The rest of this letter is organized as follows. Section II discusses the operating principles of the AWLR-based BP-to-BS concept. In Section III, a proof-of-concept demonstration is presented through single-band and dual-band BP-to-BS prototypes. Finally, the contributions of this letter are summarized in Section IV.

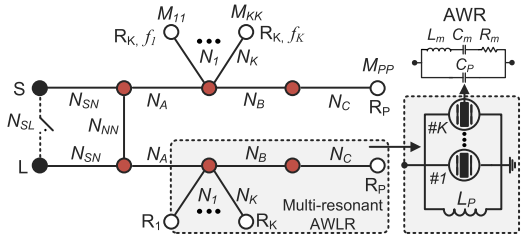

Fig. 1. CRD of a K-band AWLR-based BP-to-BS filter that exhibits reconfigurable BPF and BSF modes of operation. Black circles: source (S) and load (L). Brown circles: zero-susceptance NRNs. White circles: resonating nodes. Black solid lines: inter-node couplings. Black dashed lines: reconfigurable source-to-load coupling that controls the mode of operation. BPF mode: N_{SL} switch is open. BSF mode: N_{SL} switch is closed. The dashed area denotes the multiresonant AWLR that is shaped by K AWRs and an inductor L_P.

II. Filter Concept and Theoretical Foundations

The coupling-routing diagram (CRD) and circuit details of the AWLR-based BP-to-BS filter concept are shown in Fig. 1. It is based on two multiresonant AWLR-based modules, five static (N_{SN}, N_{NN}, and N_A) and one RF-switched (N_{SL}) impedance inverters that result in reconfigurable multiband BPF and BSF transfer functions whose bands are, respectively, shaped by two poles or two zeros. Each multiresonant AWLR comprises of K parallel-cascaded AWRs—each AWR is modeled by its Butterworth-Van-Dyke circuit model [3] in which C_m, L_m, and R_m represent its series resonant frequency and C_P represents the parasitic capacitance—whose series resonances define the center frequency of each of the K bands. From the coupling-matrix synthesis perspective, the multiresonant module is represented by $K + 1$ resonating nodes ($R_1 - R_K$ and R_P) and two nonresonating nodes (NRNs). $R_1 - R_K$ denote the K individual series resonances of the

Manuscript received November 14, 2018; revised January 1, 2019; accepted February 8, 2019. Date of publication March 28, 2019; date of current version April 8, 2019. This work was supported by the National Science Foundation under Award 1731956. *(Corresponding author: Dimitra Psychogiou).*

The authors are with the Department of Electrical, Computer, and Energy Engineering, University of Colorado at Boulder, Boulder, CO 80309 USA (e-mail: dimitra.psychogiou@colorado.edu).

Color versions of one or more of the figures in this paper are available online at http://ieeexplore.ieee.org.

Digital Object Identifier 10.1109/LMWC.2019.2901199

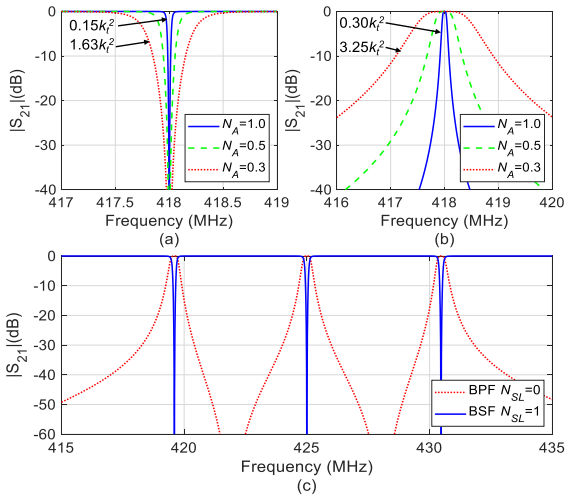

Fig. 2. Theoretically synthesized power transmission responses of the AWLR-based BP-to-BS filter using the CRD in Fig. 1 for a single-band ($K = 1$) and a triple-band ($K = 3$) example. (a) Single-band filter operating in the BSF mode ($N_{\rm SL} = 1$) for various values of N_A. (b) Single-band filter operating in the BPF mode ($N_{\rm SL} = 0$) for various values of N_A. (c) Three-band ($K = 3$) filter when operating in the BPF and BSF modes. For all responses, the rest of the normalized coupling values are $N_{\rm SN} = 1$, $N_{\rm NN} = 1$, $N_A = 0.5$, $N_B = 1.41$, $N_C = 250$, $N_1 = 1.41$, and $N_2 = N_3 = 1.41$ (triple-band only) and $M_{11} = M_{\rm PP} = 0$ and $M_{22} = -M_{33} = 80$ (triple-band only).

AWRs, whereas R_P is created by L_P and the parallel combination of the AWRs' parasitic capacitances $C_T = \sum_{n=1}^{K} C_{Pn}$ and needs to resonate at the average frequency of $f_1 - f_K$ (f_K: center frequency of band K). In this manner, the series resonance of each AWR is decoupled from its antiresonance resulting in a single high-Q pole/zero at the center frequency of each band as also discussed in [3], however, only for multi-band filters that exhibit a single BPF mode of operation. In the proposed BP-to-BS filter architecture, the mode of operation is tuned between multiband BPF and BSF by enabling and disabling $N_{\rm SL}$ which alters the source-to-load coupling.

In order to illustrate the operational principles of the multiband AWLR-based BP-to-BS concept, multiple ideally synthesized transmission responses are depicted in Fig. 2 for AWRs with $k_t^2 = 0.08\%$ (typical value for commercially available SAW resonators) and using the CRD in Fig. 1. Specifically, Fig. 2(a) and (b) shows the transmission responses of a single-band ($K = 1$) example when operating in the BSF and BPF modes, respectively, and N_A is altered. As shown, the FBW is inversely proportional to N_A. In addition, for a certain N_A value, the FBW of the BPF mode is always wider than the one of the BSF mode (e.g., 0.045% in the BSF mode and 0.09% in the BPF mode when $N_A = 0.3$). Furthermore, the FBWs of both the modes can be designed wider than k_t^2 (e.g., 1.63 k_t^2 for $N_A = 0.3$ in the BSF mode) as opposed to conventional ladder/lattice design AWR-based filters in which FBW is limited to 0.4–0.8 k_t^2 as for example in [1] and [2]. In Fig. 2(c), the synthesized BPF- and BSF-mode transmission responses of a three-band ($K = 3$) filter are illustrated showing the applicability of the proposed concept for multiband transfer functions while using less filter elements (i.e., inverters and resonators) than conventional filter banks. Note that in conventional filter banks, multiple BPFs and BSFs are combined in parallel through switches which for a K-band BP-to-BS transfer function require at least $6K$ inverters, $4K$ resonators, and multiple switches [9] as opposed to six inverters, $2K$ resonators, and one switch in this concept.

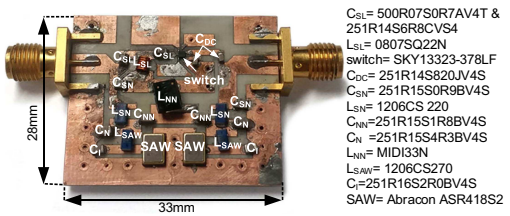

Fig. 3. Manufactured prototype of the single-band BP-to-BS filter.

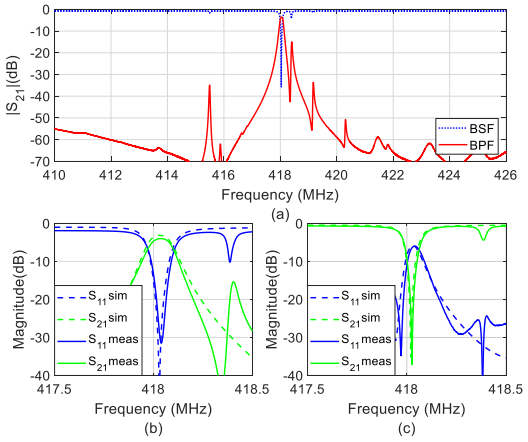

Fig. 4. RF-measured and EM-simulated S-parameters of the single-band BP-to-BS prototype in Fig. 3. (a) Power transmission response of the BPF and BSF mode. (b) Details of the BPF mode. (c) Details of the BSF mode.

III. Experimental Validation

To validate the AWLR-based BP-to-BS filter concept, two prototypes—a single-band filter at 418 MHz and a dual-band filter with bands centered at 418 and 433.9 MHz—were designed, manufactured, and measured using commercially available SAW resonators and surface-mounted lumped elements. Both the filters were built on a Rogers 4003C substrate ($\varepsilon_r = 3.38$ and $h = 1.52$ mm). Their design was completed with electromagnetic (EM) simulations in the software package Advanced Design System while taking into consideration the design principles in Section II and standard CRD to lumped-element transformations [9]. In particular, the inverters $N_{\rm SN}$ and N_A were realized with their first-order low-pass π-type circuit equivalent, whereas $N_{\rm SL}$and $N_{\rm NN}$ by their high-pass T-type equivalent. For the BPF/BSF mode selection, a single-pole double-throw switch—positioned between the output port and the $N_{\rm SL}$ inverter with its remaining port grounded—was incorporated in $N_{\rm SL}$. DC blocking capacitors ($C_{\rm DC}$) were added for the switch biasing.

The manufactured prototype of the single-band BP-to-BS filter and its constituent components are shown in Fig. 3. It was designed for a center frequency of 418 MHz and the FBWs of 0.03% and 0.04% for, respectively, the BPF and the BSF modes using the Abracon SAW resonator ASR418S2 ($C_P = 1.6$ pF, $R_m = 22.17\ \Omega$, $C_m = 1.21$ fF, and $L_m = 119.67\ \mu$H). Its measured RF response is shown in Fig. 4 along with a comparison of its corresponding EM-simulated one. In particular, Fig. 4(a) shows the filter response in a broad range, whereas Fig. 4(b) and (c) depicts the 418-MHz band details for both the modes of operation. A summary of its major RF performance metrics is provided in Table I. For both the modes of operation, $Q_{\rm eff}$ was estimated $>$ 10,000 demonstrating the applicability of the filter concept to small size and high-Q BP-to-BS filter developments.

TABLE I

SUMMARY OF MEASURED RF-PERFORMANCE PARAMETERS

Filter	f_{cen}, MHz	Mode	BW, kHz	xk_t^2	IL, dB
Single-band	418	BSF	116	0.36	38.5
Single-band	418	BPF	137	0.43	4.0
Dual-band	418	BSF	106	0.33	26.8
Dual-band	418	BPF	332	1.03	1.5
Dual-band	433.9	BSF	194	0.49	27.2
Dual-band	433.9	BPF	507	1.26	1.2

f_{cen}: center frequency of band, IL: insertion loss at f_{cen}

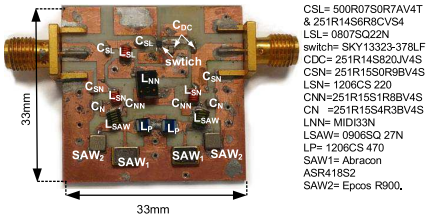

Fig. 5. Manufactured prototype of the dual-band BP-to-BS filter.

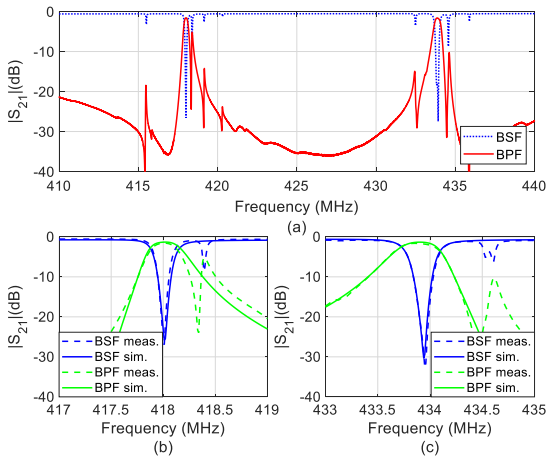

Fig. 6. RF-measured and EM-simulated power transmission response of the prototype in Fig. 5. (a) BPF and BSF modes. (b) Details of the lower band for the BPF and BSF modes. (c) Details of the upper band for the BPF and BSF modes.

The manufactured prototype of the dual-band BP-to-BS filter is depicted in Fig. 5. For its design, the commercially available SAW resonators from Abracon (ASR418S2) and Epcos (R900 with $C_P = 1.62$ pF, $R_m = 19\ \Omega$, $C_m = 1.62$ fF, and $L_m = 83\ \mu$H) were used. A comparison of its RF-measured and simulated transfer functions is shown in Fig. 6 for a broad frequency range [see Fig. 6(a)] as well as around the two bands of interest [see Fig. 6(b) and (c)] for both the BPF and BSF modes. As it can be seen, they are in good agreement with each other validating the suitability of the devised filter concept for multiband BP-to-BS realizations. Furthermore, Table I provides a summary of the performance metrics of the dual-band prototype and validates the suitability of the multiband BP-to-BS concept for FBWs that are not limited by k_t^2. In addition, for all measured states, low IL levels can be observed in the two passbands of the BPF mode and in the out-of-band passband areas of the BSF mode of operation which correspond to the values of Q_{eff} above 10,000. A comparison between the BP-to-BS prototype and other AWR-based filters is summarized in Table II. It reveals that the proposed concept is the only one that allows the realization of BP-to-BS responses within the same filter volume while retaining the highest Q_{eff}, lowest IL, and wider FBW than conventional AWR filters.

TABLE II

COMPARISON WITH STATE-OF-THE-ART

Ref.	f_{cen}, GHz	Bands (order)	Resp.	FBW xk_t^2	IL, dB	Tech.	Q_{eff}
This work	0.418/ 0.433	2 (2)	BS BP	1.03 1.26	26.8 1.5	SAW	>10k
[3]*	0.418/ 0.433	2 (2)	BP	0.6- 1.9	3.3- 1.2	SAW	>10k
[5]*	2.08	1(3)	BP AS	0.43	2.3 14	BST- FBAR	230
[6]	5.49	1 (3)	BP	1.03	13	GaN	700
[7]	1.3/1.6	2 (9)	BP	0.49	27.2	BAW	1200
[8]*	0.246	1 (1)	BP AS	N/A	57 76	AlGaN	608

*Reconfigurable, BS: bandstop, BP: bandpass, AS: all-stop

IV. CONCLUSION

This letter addressed the RF design and practical development of a new class of reconfigurable AWLR-based RF filters for multiband BP-to-BS transfer function characteristics. They are based on multiresonant modules that are shaped by in-parallel cascaded AWLRs and a reconfigurable source-to-load coupling. The proposed BP-to-BS concept was experimentally validated through single-band and dual-band prototypes that demonstrated the BPF and BSF modes of operation with passbands/stopbands exhibiting FBWs wider than conventional ladder/lattice AWR-based BPFs and high values of Q_{eff}.

REFERENCES

[1] C. C. W. Ruppel, "Acoustic wave filter technology—A review," *IEEE Trans. Ultrason., Ferroelectr., Freq. Control*, vol. 64, no. 9, pp. 1390–1400, Sep. 2017.

[2] S. Gong and G. Piazza, "Design and analysis of lithium–niobate-based high electromechanical coupling RF-MEMS resonators for wideband filtering," *IEEE Trans. Microw. Theory Techn.*, vol. 61, no. 1, pp. 403–414, Jan. 2013.

[3] D. Psychogiou, R. Gómez-García, and D. Peroulis, "Single and multiband acoustic-wave-lumped-element-resonator (AWLR) bandpass filters with reconfigurable transfer function," *IEEE Trans. Microw. Theory Techn.*, vol. 64, no. 12, pp. 4394–4404, Dec. 2016.

[4] D. Psychogiou, R. Gómez-García, and D. Peroulis, "Acoustic wave resonator-based absorptive bandstop filters with ultra-narrow bandwidth," *IEEE Microw. Wireless Compon. Lett.*, vol. 25, no. 9, pp. 570–572, Sep. 2015.

[5] M. Z. Koohi, S. Lee, and A. Mortazawi, "Fabrication of a low insertion loss intrinsically switchable BAW filter based on BST FBARs," in *IEEE MTT-S Int. Microw. Symp. Dig.*, Honolulu, HI, USA, Jun. 2017, pp. 1480–1483.

[6] D. Neculoiu, A.-C. Bunea, A. M. Dinescu, and L. A. Farhat, "Band pass filters based on GaN/Si lumped-element SAW resonators operating at frequencies above 5 GHz," *IEEE Access*, vol. 6, pp. 47587–47599, 2018.

[7] Y. Sun, Q. Yang, H. Zhang, D. Zhang, and W. Pang, "A compact dual-passband filter based on bulk acoustic wave technology," in *IEEE MTT-S Int. Microw. Symp. Dig.*, Phoenix, AZ, USA, May 2015, pp. 1–4.

[8] L. C. Popa and D. Weinstein, "Switchable piezoelectric transduction in AlGaN/GaN MEMS resonators," in *Proc. 17th Intern. Conf. Solid-State Sensors, Actuat. Microsyst.*, Barcelona, Spain, Jun. 2013, pp. 2461–2464.

[9] J.-S. G. Hong, *Microstrip Filters for RF / Microwave Applications*, 2nd ed. Hoboken, NJ, USA: Wiley, 2011.